Journal of Power Sources 205 (2012) 525–529

Contents lists available at SciVerse ScienceDirect

Journal of Power Sources

journal homepage: www.elsevier.com/locate/jpowsour

Short communication

Highly oriented hematite nanorods arrays for photoelectrochemical water splitting

Vitor A.N. de Carvalho[a], Roberto A. de S. Luz[a], Bruno H. Lima[b], Frank N. Crespilho[a,c], Edson R. Leite[b], Flavio L. Souza[a,*]

[a] Centro de Ciências Naturais e Humanas, Grupo de Materiais e Métodos Avançados - Universidade Federal do ABC, CEP 09090-400, Santo André, SP, Brazil
[b] PPGCEM – Universidade Federal de São Carlos, CEP 13565-905, São Carlos, SP, Brazil
[c] Instituto de Química de São Carlos, CP 780, 13560-970 São Carlos, SP, Brazil

ARTICLE INFO

Article history:
Received 16 December 2011
Received in revised form 9 January 2012
Accepted 12 January 2012
Available online 21 January 2012

Keywords:
Iron oxide
Nanorod array
Electrochemical properties
Water splitting

ABSTRACT

We report an oriented hematite undoped photanode synthesized by single chemical route step at low temperature and with a short reaction time. Fluorine-doped tin oxide (FTO) electrodes modified with hematite nanorod (450 nm of thickness) showed a photocurrent with 0.9 mA cm^{-2} at 0.4 V *vs* Ag/AgCl. Also, we have done electrochemical characterizations under dark conditions in order to understand the catalytic properties of the photoanode. Based on cyclic voltammetry results we have proposed a new mechanism to explain the evolution of molecular oxygen onto oriented hematite surfaces, in which is not inconsistent with thermodynamical parameters extracted from the Pourbaix diagram. A chemical interaction between OH^- and iron oxide from the surface suggested that the chemical reaction is first governed by oxy-hydroxides on the electrode/electrolyte interface. In other word, molecular oxygen evolution is preceded by the formation of oxy-hydroxide groups, a slow and possibly limiting step.

1. Introduction

Iron oxide, in the hematite phase (α-Fe_2O_3), remains an excellent candidate to be applied as a photoanode in a photoelectrochemical (PEC) water splitting cell due to its abundance, high electrochemical stability, low toxicity, environmental compatibility, its suitable band gap (optimum absorption in visible light range, E_g = 2.2 eV) [1] and valence band edge position. Nevertheless, hematite presents a short excited state lifetime (10 ps) [2], an unfavorable band position for unassisted water splitting, and a small hole diffusion length (2–4 nm) [3], compromising its performance. Recently, several nanoarchitectures have been proposed [4–32] to build photoelectrochemical electrodes from hematite. However, the optimized hematite performances are far from the best value demonstrated by the theoretical calculation for this material [12]. Grätzel and coworkers [4–7] have reported many improvements in different nanostructured hematites; more recently, they showed a new photocurrent density record (2.9 mA cm^{-2} at +1.23 V *vs* RHE) [19] using iridium oxide doped-hematite film for splitting water. Although many authors have contributed to the understanding of phenomena at the interface of nanomaterial-hematite/electrolyte [33–37], there is still an important question: what is the real electrochemical mechanism that explains the effect of hematite-front electrocatalytic evolution of oxygen? In order to contribute to answer this question, the present paper report for the first time a new evidence that the mechanism of oxidation of hydroxyl ions occur by two stages of reaction at hematite nanorods, the first being the formation of iron hydroxides (adsorption of OH^-), followed by electro-oxidation. This approach suggests an additional pathway to the commonly model stated in the literature for nanostructured hematite [1–36], in which the photoelectrochemical reactions for water splitting is frequently (and shortly) showed by the collect electrons via the outersphere reaction of OH^- onto electrode surface. Also, the electrochemical properties of hematite nanorods have been less studied, with attention predominantly focused random nanoparticulate network (RNN) applications, mainly for nanocrystalline TiO_2 modified electrodes.

2. Experimental

2.1. Synthesis of highly oriented hematite nanorods

In a typical procedure, all chemical reactants commercially available (analytical grade) were used without further purification steps. Our strategy is based on the work of Vayssieres [16], which proposes a synthetic route to prepare highly oriented α-Fe_2O_3 nanorod arrays by controlled aqueous growth. Following a typical procedure, 95 mL of aqueous solution (deionized water with resistivity greater than 15 MΩ cm^{-1}) containing 0.15 mol L^{-1} ferric chloride ($FeCl_3 \cdot 9H_2O$, Mallinckrodt, 97%) and 1 mol L^{-1} sodium

* Corresponding author. Tel.: +55 11 4996 8353; fax: +55 11 4996 0090.
E-mail address: fleandro.ufabc@gmail.com (F.L. Souza).

0378-7753/$ – see front matter © 2012 Elsevier B.V. All rights reserved.
doi:10.1016/j.jpowsour.2012.01.093

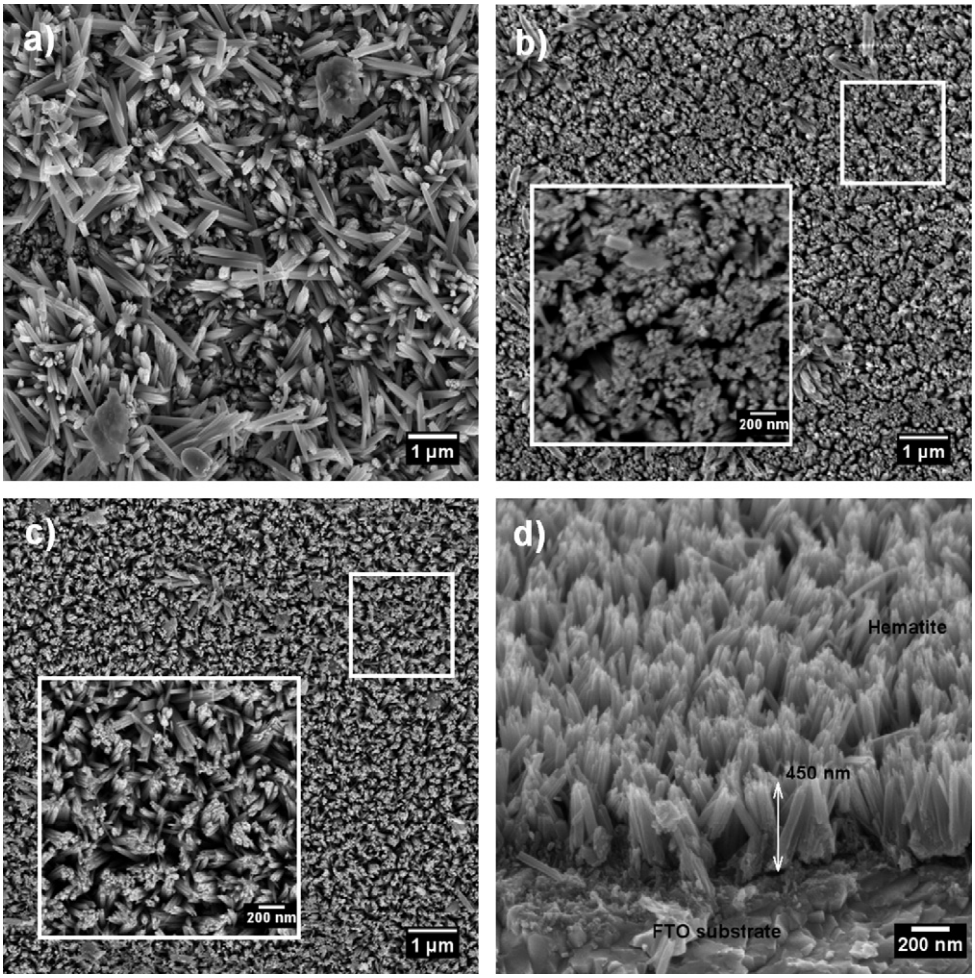

Fig. 1. SEM–FEG image from the top-view of an undoped hematite nanostructured film. (a) The sample was prepared without any treatment on the substrate (FTO) surface during 24 h by the PBM route, (b) the sample after the heat treatment 24 h and carefully cleaned substrate surface (FTO), (c) top-view SEM–FEG images of the undoped FTO–hematite nanostructured film and (d) cross-sectional view of the film. Both (c) and (d) samples were prepared during 6 h by the PBM route on FTO (commercial, fluorine-doped tin oxide layer with 520 nm thickness).

nitrate ($NaNO_3$, Merck, 99,5%) at pH 1.5 (by HCl, Nuclear, 36.5–40%). This solution was poured into a bottle with an autoclavable screw cap. The polycrystalline conductor fluorine-doped tin oxide glass substrates (FTO-Flexitec, R_Ω = 10–15 Ω cm^{-1}) of interest were placed in the bottle in the vertical position. The bottle was then placed in a regular laboratory oven and subjected to a constant temperature (100° C) for 6 h. After the growth process, the substrates were washed in distilled water in an ultrasonic bath to remove any residual salts and allowed to dry in air at room temperature. The mixed phases, such as akaganeite, goethite and hematite, were the first phases obtained, and an additional heat treatment in air at 390 °C for 1 h was required to obtain a pure thermodynamically stable crystallographic phase of ferric oxide (i.e., hematite), skillfully designed with the required nanorod morphology. It is important to mention that for all analysis, the samples were investigated after the photoelectrochemical measurements and the sample positions coincided with the illuminated area.

2.2. Characterization of hematite nanorods modified FTO electrodes

The crystalline phases of nanorods films and powders (before and after the heat treatment) were identified by XRD (Rigaku D-Max 200, using Cu Ka radiation) with the rotary anode operating at 150 kV and 40 mA in the 2θ range from 10° to 80° with a step scan of 0.02°, 12 s per step, and the optical characterization of the film was performed by a Cary 5E UV–vis spectrophotometer. The film morphology and thickness (by cross-sectional analysis of the cleaved sample) were characterized by FE–SEM (Zeiss Supra 35).

2.3. Electrochemical and photoelectrochemical experiments

The electrochemical and photoelectrochemical measurements were carried out in a standard three-electrode cell using the hematite film as the working electrode (1.0 cm^2 area), Ag/AgCl in a KCl-saturated solution as the reference electrode and platinum wire as the counter electrode. A 1.0 mol L^{-1} NaOH (Vetec, 99%) and 0.1 mol L^{-1} KCl (Merk pro-analysis in high-purity water, pH = 13.6 and pH 7.0) solution were used as the electrolytes. A scanning potentiostat (Potentiostat/Galvanostat μAutolab III) was used to measure the dark and illumination currents at a scan rate of 50 mV s^{-1}. Sunlight (1000 W m^{-2}) was simulated with a 450 W xenon lamp (Osram, ozone free) and an AM 1.5 filter. The light intensity was set to 100 mW cm^{-2}.

3. Results and discussion

The highly oriented 3D array of α-Fe_2O_3 nanorod is achieved by modifying the strategy (Fig. 1a and b, reproducing the original strategy) developed by Vayssieres [16–18], called “purpose-built

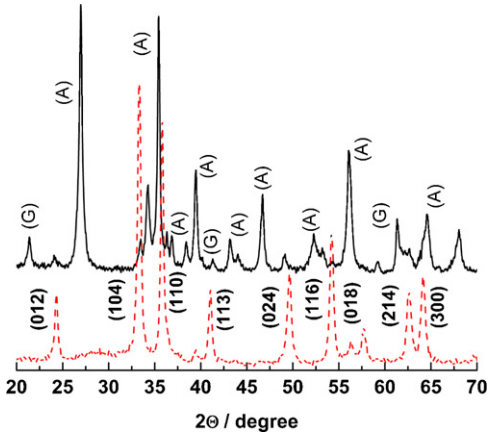

Fig. 2. X-ray results of the samples synthesized by the PBM route. The solid black line is the XRD curve identified with letters G and A, corresponding to two different hydrated phases of iron oxide, Goethite and Akaganeite. The dashed red line is the curve identified by the crystallography planes, providing information about iron oxide in the hematite phase (α-Fe_2O_3). All of the samples analyzed were supported on the conductor substrate (layer with 520 nm thickness, fluorine-doped SnO_2). (For interpretation of the references to color in this figure legend, the reader is referred to the web version of the article.)

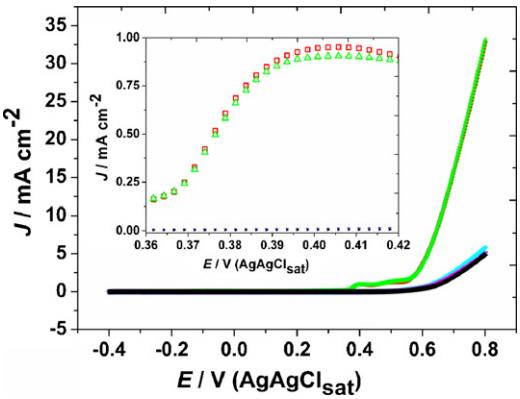

Fig. 3. Photocurrent density *vs* voltage measured (three electrode set-up, in aqueous NaOH, pH 13.6) in dark (curve black and light blue) and illuminated conditions under a sunlight simulator with a 1.5-AM global filter (green (Δ) and (□) red dots). The inset highlights the plateau of the beginning of the O_2 evolution (0.37 V) on the photoanode (FTO–hematite film). (For interpretation of the references to color in this figure legend, the reader is referred to the web version of the article.)

materials" (PBM). The main difference in our experiment is that we obtained a 3D array of α-Fe_2O_3 nanorods within 6 h of synthesis, using a different process for cleaning and heat treatment of the FTO surfaces, which resulted in nanorods with high orientation and homogeneity of distribution (Fig. 1c and d). Fig. 1d shows the cross-section of the FTO–hematite electrode, in which the thickness is estimated to be 450 nm. Additionally, we clearly observed the vertically oriented hematite nanorod arrays on the FTO. X-ray diffraction (XRD) of the film, shown in Fig. 2 (red and black lines), exhibits the formation of hematite (α-Fe_2O_3) and akaganeite/goethite (FeOOH) phase superimposed on FTO glass substrate pattern. The peaks were identified using the JCPDS catalog as reference with a standard values. The peaks not identified in Fig. 2 are ascribed to SnO_2 (cassiterite phase) from the fluorine-doped SnO_2 (FTO) substrate. The optical properties showed strong absorption in the visible region for the α-Fe_2O_3 nanorods films (data not shown). From this data the indirect and direct electronic band *gap* was calculated considering the following equation $(\alpha h\nu) = A_o(h\nu - E_g)^m$, where $h\nu$ is the photon energy (in eV), E_g is the optical band gap energy (in eV) and A_o and m are constant, which depend on the kind of electronic transition, where m is equal to 1/2 for a direct allowed and 2 for an indirect forbidden transition. The values estimated were 1.95 and 2.1 eV, respectively, in good agreement with the literature [1–21].

Fig. 3 shows the photocurrent generated under illuminated and dark conditions, using the three-electrode configuration cell ($Ag/AgCl_{sat}$ as the reference electrode and Pt plate as the auxiliary electrode) in aqueous solution of NaOH (pH 13.6) and KCl (pH 7.0). Under dark conditions, a low catalytic current was observed in the anodic region. When the systems were illuminated using a sunlight simulator (free ozone Xenon Lamp, 100 mW m^{-2} with AM 1.5 global), the photocurrent was 0.9 mA cm^{-2} in 0.37 V *vs* $Ag/AgCl_{sat}$, with a maximum value of 3.0 mA cm^{-2} in 0.6 V *vs* $Ag/AgCl_{sat}$ in aqueous NaOH (pH 13.6). For the latter, we clearly see the enhancement achieved comparing with the seminal work reported by Vayssieres and co-workers; 2.0 and 11.0 μA cm^{-2} at 0.37 and 0.6 V *vs* $Ag/AgCl_{sat}$, respectively [17,18]. The hematite photoanode was also performed at neutral aqueous solution (KCl, pH 7.0) and no significant shift between photocurrent in dark-illuminated condition was observed (data not shown). Indeed, this behavior is expected occur when the hematite photoresponse are measured at neutral environment as pointed out by others authors [17].

As observed in the FE–SEM images, the FTO–hematite electrodes have a high surface area, enabling excellent transport of holes to the semiconductor surface. It is well known that because hematite is usually an *n*-type semiconductor, the Fermi energy in hematite is closer in energy to the conduction band than to the valence band.

To better understand how to occur the formation of molecular oxygen on the surface of hematite some experiments in dark conditions were carried out in order to observe changes in the voltammetric profile of the modified FTO electrode. For this, we cycled FTO–hematite electrode for several times (more than 100 cycles, see inset Fig. 4a) through a basic medium (pH 13.6) with a potential window ranging from 0.8 to −0.8 V in the dark (Fig. 4a–c). In this potential range, there is clearly an irreversible reduction peak at −0.5 V (Fig. 4a). By varying the scan rate (ν), it was observed that the electrochemical reaction is limited by charge-transfer [38–40] up to 500 mV s^{-1} in the *I vs* ν plot (Fig. 4d), showing that the electrochemical process originates from the adsorbed groups at the surface of the nanorods. Based on the Pourbaix diagram for bulk electrode [41,42], iron hydroxide can be formed simultaneously with the reduction of Fe(III) to Fe(II). Interestingly, this process appears only if the electrochemistry follows an anodic pathway (inset Fig. 4b); otherwise, this process slowly disappears, revealing consumption of these species at the surface. It is worth mentioning that the effect in the cathode region has been the subject of many studies [43–55]. Similar to cathodic peak founded here, it has been observed in TiO_2 electrodes (in context of dye-sensitized solar cells), which is attributed to charging of surface states, when there is also the chemical capacitance in the semiconductor, and space charge capacitance [54].

Several effects in cathodic region has been reported for nanostructured TiO_2 films [43–55], showing several characteristic features, in which the dominant ones has been related to exponential density of states (DOS) at the negative potentials approaching the conduction band potential. Bisquert et al. [54] reported that the symmetric and much less intense peak appears at less negative potentials (similarly to the hematite at −0.8 V region), and these features are highly symmetric with respect to voltage axis in good quality electrodes, though they sometimes appear as a distortion due to IR drop. Also, it was reported that for very negative potentials scan, where the electrochemical potential is close to the conduction band edge, the capacitance is controlled by both Helmholtz capacitance at the inner surface and the film enters into band unpinning [54,56]. Furthermore, an additional peak at a more positive potential can appear (in our case, for hematite at −0.5 V), that it was well

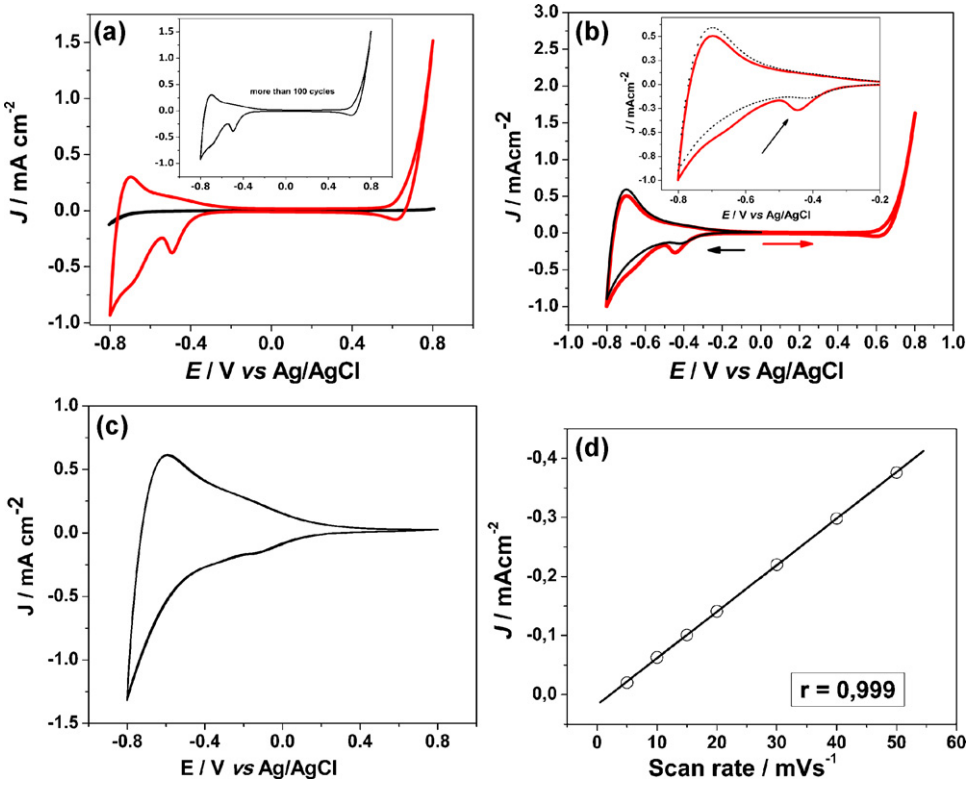

Fig. 4. Cyclic voltammograms under dark conditions at pH 13.6 (NaOH) of the, (a) FTO electrode (black line (—)) and FTO–hematite (red line ( )); Inset. FTO–hematite performance during more than 100 cycles of stability, (b) FTO–hematite electrode (black line) measured at a negative potential and FTO–hematite at a positive potential (red line). Inset: Zoomed in image of the FTO–hematite in the negative region. (c) FTO–hematite at pH 7.0 (KCl). All of the measurements were performed at 50 mV s^{-1} (23 °C ± 0.1 °C) and (d) linear fitting of Current density (*J*) *vs* scan rate (ν) of FTO–Fe_2O_3 films at pH 13.6. Electrolyte: NaOH 0.1 mol L^{-1}. (For interpretation of the references to color in this figure legend, the reader is referred to the web version of the article.)

established experimentally for nanostructured TiO_2 films in 1995 by Grätzel and co-workers [43].

The peaks at the more positive potentials have been reported for in TiO_2 random nanoparticulate network, in which it are characteristic for nanostructured films and have not been obtained in polycrystalline electrodes [57]. Boschloo and Fitzmaurice [44] reported the cyclic voltammetry of a nanostructured TiO_2 electrode (aqueous $LiClO_4$, pH 6.2), when after 15 min stabilization at +0.80 V, the potential was scanned to −0.80 V and a small current peak was observed in the forward scan at −0.38 V. The size of this peak decreased significantly when a second cyclic potential scan was performed directly afterward. For this case, the authors claimed that the small current maximum is due to filling of surface states and the subsequent increase in conductivity, suggesting that it is probably due to the fact that once the nanocrystals close to the back contact become depleted of electrons, the rest of the film is isolated from the applied potential. In another approach, Kavan et al. [43] ascribed this effect to the chemisorption of water on TiO_2. It is well-known that anatase TiO_2 contains surface OH groups, but they can be almost completely removed at 400 °C. Based on the latter, the authors used dehydroxylated electrodes and observed that the passage of a cathodic current caused the reduction of trace water, which induces a series of chemical reactions.

Thus, for hematite nanorods we have assumed that OH^- groups adoption on hematite surface show an electrochemical behavior governed by a Nernstian equilibrium, similarly to the Nernstian H^+/OH^- equilibrium reported to nanostructured TiO_2 films [58,59]. This is a strong indication that the electrocatalytic anodic process for molecular oxygen evolution is also undergoing a structural rearrangement step, in which some species of Fe(III) in the crystalline structure of hematite have different energy from those present in the bulk nanorods. For the latter assumption, this effect should only occur in basic media, once the OH^- ions are directly associated with the reaction mechanism. To verify this, we performed the same experiment, but in neutral KCl at 0.1 mol L^{-1}. As can be seen in Fig. 4c, no changes in the voltammetry profile were observed; only a decrease in the capacitive currents is observed in this case.

Thus, we suggest the presence of an intermediate slow step, in which Fe(III) forms an oxide/hydroxide intermediate before the molecular oxygen evolution. Therefore, the complete mechanism proposed here for oxygen evolution on hematite nanorod film is shown in Eqs. (1) and (2).

Step 1: OH^- adsorption (*slow*)

$$4\alpha\text{-}Fe_2O_3 + 4OH^- \rightarrow 4\alpha\text{-}Fe_2O_3(OH)^-_{ads} \quad (1)$$

Step 2: molecular oxygen evolution ($E = 0.38$ V)

$$4\alpha\text{-}Fe_2O_3(OH)^-_{ads} + 4h\nu \rightarrow 4\alpha\text{-}Fe_2O_3 + \uparrow O_2 + 2H^+ + 2H_2O + 2e^- \quad (2)$$

Besides this additional step considering a slow intermediate reaction (formation of oxide/hydroxide) before the molecular oxygen evolution, it worth mentioned that the others elementary steps in the detailed mechanism are far from known. The mechanism proposed here is a part of several others mechanisms for different materials found in literature [60–70]. For instance, based on Tafel slopes, Trasatti [67] suggested that molecular oxygen is liberated from two highly oxidized sites presents onto semiconductor surface. However, the latter proposed mechanism does not make any distinction between the intermediate oxygen that arises from the oxide lattice and from water species. In the case of hematite nanorods, both effects appear to be evident, in which the OH^- arise

from the solution and formation of oxide/hydroxide play important roles for water splitting.

4. Conclusion

In this work we have shown a novel approach to build hematite nanorods onto FTO surfaces and the implications for photoelectrochemical water splitting. We obtained a 3D array of α-Fe_2O_3 nanorods within 6 h of synthesis, when the systems (hematite nanorods film with 450 nm of thickness) were illuminated using a sunlight simulator, and the photocurrent obtained was 0.9 mA cm^2 at 0.4 V with a maximum value of 3.0 mA cm^2 at 0.6 V. We propose that the evolution of molecular oxygen is preceded by the formation of oxy-hydroxide groups, a slow and possibly limiting step. This proposes is not inconsistent with thermodynamical parameters extracted from the Pourbaix diagram for bulk material. A chemical interaction between OH^- and iron oxide from the surface suggested that the chemical reaction is first governed by oxy-hydroxides on the electrode. The capacitive currents at −0.8 V region were observed, and it is very similar to the concept of pseudocapacitance in the random nanoparticulate network [54]. We have assumed that OH^- groups adoption on hematite surface show an electrochemical behavior governed by a Nernstian equilibrium, similarly to the Nernstian H^+/OH^- equilibrium reported to nanostructured TiO_2 films.

Acknowledgements

We gratefully acknowledged financial support from the Brazilian agencies of FAPESP (Grant No. 2010/02464-6, 09/15558-1 and 2011/01541-0), CAPES, CNPq (555855/2010-4), Instituto Nacional em Eletrônica Orgânica (INEO), NanoBioMed Brazil Network (CAPES) and INCTMN.

References

[1] T. Lindgren, L. Vayssieres, H. Wang, S.E. Lindquist, Chem. Phys. Nanostruct. Semicond. 83 (2003) 83–110.
[2] J.H. Kennedy, K.W. Frese, J. Electrochem. Soc. 125 (1978) 709–714.
[3] N.J. Cherepy, D.B. Liston, J.A. Lovejoy, H.M. Deng, J.Z. Zhang, J. Phys. Chem. B 102 (1998) 770–776.
[4] I. Cesar, A. Kay, J.A.G. Martinez, M. Grätzel, J. Am. Chem. Soc. 128 (2006) 4582–4583.
[5] K. Sivula, F.L. Formal, M. Grätzel, Chem. Mater. 21 (2009) 2862–2867.
[6] I. Cesar, K. Sivula, A. Kay, R. Zboril, M. Grätzel, J. Phys. Chem. C 113 (2008) 772–782.
[7] K. Sivula, R. Zboril, F.L. Formal, R. Robert, A. Weidenkaff, J. Tucek, J. Frydrych, M. Grätzel, J. Am. Chem. Soc. 132 (2010) 7436–7444.
[8] B.I. Kharisov, O.V. Kharissova, M.J. Yacaman, Ind. Eng. Chem. Res. 49 (2010) 8289–8309.
[9] J. Sun, D.K. Zhong, D.R. Gamelin, Energy Environ. Sci. 3 (2010) 1252–1261.
[10] L. Andrade, R. Cruz, H.A. Ribeiro, A. Mendes, Int. J. Hydrogen Energy 35 (2010) 8876–8883.
[11] J. Frydrych, L. Machala, M. Hermanek, I. Medrik, M. Mashlan, J. Tucek, J. Pechousek, V.K. Sharma, Thin Solid Films 518 (2010) 5916–5919.
[12] N.T. Hahn, H. Ye, D.W. Flaherty, A.J. Bard, C.B. Mullins, ACS Nano 4 (2010) 1977–1986.
[13] F.L. Souza, K.P. Lopes, P.A.P. Nascente, E.R. Leite, Sol. Energy Mater. Sol. Cells 93 (2009) 362–368.
[14] F.L. Souza, K.P. Lopes, E. Longo, E.R. Leite, Phys. Chem. Chem. Phys. 11 (2009) 1215–1219.
[15] A.B. Murphy, P.R.F. Barnes, L.K. Randeniya, I.C. Plumb, I.E. Grey, M.D. Horne, J.A. Glasscock, Int. J. Hydrogen Energy 31 (2006) 1999–2017.
[16] L. Vayssieres, N. Beermann, S.E. Lindquist, A. Hagfeldt, Chem. Mater. 13 (2001) 233–235.
[17] N. Beermann, L. Vayssieres, S.E. Lindquist, A. Hagfeldt, J. Electrochem. Soc. 147 (2000) 2456–2461.
[18] T. Lindgren, H. Wang, N. Beermann, L. Vayssieres, S.E. Lindquist, A. Hagfeldt, Sol. Energy Mater. Sol. Cells 71 (2002) 231–243.
[19] S.D. Tilley, M. Cornuz, K. Sivula, M. Grätzel, Angew. Chem. Int. Ed. 49 (2010) 6405–6408.
[20] Y. Li, J.Z. Zhang, Laser Photon. Rev. 4 (2009) 517–528.
[21] A.A. Tahir, K.G. Upul Wijayantha, S.S. Yarahmadi, M. Mazhar, V. McKee, Chem. Mater. 21 (2009) 3763–3772.
[22] F.L. Formal, N. Tétreault, M. Cornuz, T. Moehl, M. Grätzel, K. Sivula, Chem. Sci. 2 (2011) 737–743.
[23] B.M. Klahr, T.W. Hamann, J. Phys. Chem. C 115 (2011) 8393–8399.
[24] K.J. McDonald, K.S. Choi, Chem. Mater. 23 (2011) 1686–1693.
[25] R.L. Spray, K.J. McDonald, K.S. Choi, J. Phys. Chem. C 115 (2011) 3497–3506.
[26] Y. Lin, S. Zhou, S.W. Sheehan, D. Wang, J. Am. Chem. Soc. 133 (2011) 2398–2401.
[27] K. Sivula, F.L. Formal, M. Grätzel, ChemSusChem 4 (2011) 432–449.
[28] S.R. Pendlebury, M. Barroso, A.J. Cowan, K. Sivula, J. Tang, M. Grätzel, D. Klug, J.R. Durrant, Chem. Commun. 47 (2011) 716–718.
[29] K.G.U. Wijayantha, S.S. Yarahmadi, L.M. Peter, Phys. Chem. Chem. Phys. 13 (2011) 5264–5270.
[30] D.K. Zhong, M. Cornuz, K. Sivula, M. Grätzel, D.R. Gamelin, Energy Environ. Sci. 4 (2011) 1759–1764.
[31] H. Dotan, K. Sivula, M. Grätzel, A. Rothschild, S.C. Warren, Energy Environ. Sci. 4 (2011) 958–964.
[32] J. Chen, L. Xu, W. Li, X. Gou, Adv. Mater. 17 (2005) 582–586.
[33] R.V. Krol, Y. Liang, J. Schoonman, J. Mater. Chem. 18 (2008) 2311–2320.
[34] K. Itoh, J.O. Bockris, J. Electrochem. Soc. 131 (1984) 1266–1271.
[35] N.J. Cherepy, D.B. Liston, J.A. Lovejoy, H. Deng, J.Z. Zhang, J. Phys. Chem. B 102 (1998) 770–776.
[36] J. Moser, M. Grätzel, Helv. Chim. Acta 65 (1982) 1436–1444.
[37] R.F.G. Gardner, F. Sweett, D.W. Tanner, J. Phys. Chem. Solids 24 (1963) 1183–1186.
[38] W.S. Alencar, F.N. Crespilho, V. Zucolotto, O.N. Oliveira Jr., W.C. Silva, J. Phys. Chem. C 111 (2007) 12817–12821.
[39] F.N. Crespilho, M.E. Ghica, C.G. Caridade, O.N. Oliveira Jr., C. Brett, Talanta 76 (2008) 922–928.
[40] C.M.A. Brett, A.M.O. Brett, Electrochemistry Principles, Method and Applications, Oxford University Press, New York, 1993.
[41] S.H. Drissi, R.M. Abdelmoula, J.M.R. Génin, Corros. Sci. 37 (1995) 2025–2041.
[42] B. Berverskog, I. Puigdomenech, Corros. Sci. 38 (1996) 2121–2135.
[43] L. Kavan, K. Kratochvilova, M. Grätzel, J. Electroanal. Chem. 394 (1995) 93–102.
[44] G. Boschloo, D. Fitzmaurice, J. Phys. Chem. B 103 (1999) 2228–2231.
[45] H. Wang, J.H.G. Boschloo, H. Lindstrom, A. Hagfeldt, S.E. Lindquist, J. Phys. Chem. B 105 (2001) 2529–2533.
[46] F. Fabregat-Santiago, I. Mora-Seró, G. Garcia-Belmonte, J. Bisquert, J. Phys. Chem. B 107 (2003) 758–768.
[47] J. Bisquert, Phys. Chem. Chem. Phys. 5 (2003) 5360–5364.
[48] H. Randriamahazaka, F. Fabregat-Santiago, A. Zaban, J. García-Cañadas, G. Garcia-Belmonte, J. Bisquert, Phys. Chem. Chem. Phys. 8 (2006) 1827–1833.
[49] S. Tirosh, T. Dittrich, A. Ofir, L. Grinis, A. Zaban, J. Phys. Chem. B 110 (2006) 16165–16168.
[50] G.K. Mor, O.K. Varghese, M. Paulose, K. Shankar, C.A. Grimes, Sol. Energy Mater. Sol. Cells 90 (2006) 2011–2075.
[51] M. Law, L.E. Greene, A. Radenovic, T. Kuykendall, J. Liphardt, P. Yang, J. Phys. Chem. B 110 (2006) 22652–22663.
[52] I. Mora-Seró, F. Fabregat-Santiago, B. Denier, J. Bisquert, R. Tena-Zaera, J. Elias, C. Lévy-Clement, Appl. Phys. Lett. 89 (2006) 203117–203119.
[53] J. Bisquert, Phys. Chem. Chem. Phys. 10 (2008) 49–72.
[54] J. Bisquert, F. Fabregat-Santiago, I. Mora-Seró, G. Garcia-Belmonte, E.M. Barea, E. Palomares, Inorg. Chim. Acta 361 (2008) 684–698.
[55] J. Bisquert, J. Phys. Chem. Chem. Phys. 13 (2011) 4679–4685.
[56] J. Bisquert, Z. Zabn, Appl. Phys. A 77 (2003) 507–514.
[57] W.H. Leng, Z. Zhang, Z.Q. Zhang, C.N. Cao, J. Phys. Chem. B 109 (2005) 15008–15023.
[58] S. Levine, A.L. Smith, Discuss. Faraday Soc. 52 (1971) 290–301.
[59] T.W. Healy, L.R. White, Adv. Colloid Interface Sci. 9 (1978) 303–345.
[60] M.G. Walter, E.L. Warren, J.R. McKone, S.W. Boettcher, Q. Mi, E.A. Santori, N.S. Lewis, Chem. Rev. 110 (2010) 6446–6473.
[61] T.R. Cook, D.K. Dogutan, S.Y. Reece, Y. Surendranath, T.S. Teets, D.G. Nocera, Chem. Rev. 110 (2010) 6474–6502.
[62] J.O. Bockris, A. Huq, R. Proc, Proc. R. Soc. Lond. A 237 (1956) 277–296.
[63] D.K. Zhong, D.R. Gamelin, J. Am. Chem. Soc. 132 (2010) 4202–4207.
[64] D.A. Lutterman, Y. Surendranath, D.G. Nocera, J. Am. Chem. Soc. 131 (2009) 3838–3839.
[65] M.W. Kanan, D.G. Nocera, Science 321 (2008) 1072–1075.
[66] E.M.P. Steinmiller, K.S. Choi, Proc. Natl. Acad. Sci. U.S.A. 106 (2009) 20633–20636.
[67] S. Trasatti, in: J. Lipkowski, P.N. Ross (Eds.), Electrochemistry of Novel Materials, VCH Publishers, New York, 1994.
[68] M. Wohlfahrt-Mehrens, J. Heitbaum, J. Electroanal. Chem. 237 (1987) 251–260.
[69] J. Willsau, O. Wolter, J. Heitbaum, J. Electroanal. Chem. 195 (1985) 299–306.
[70] D.B. Hibbert, C.R. Churchill, J. Chem. Soc., Faraday Trans. 80 (1984) 1965–1975.